technologies

MDPI

Article

Injectable Hydrated Calcium Phosphate Bone-like Paste: Synthesis, In Vitro, and In Vivo Biocompatibility Assessment

Anastasia Yu. Teterina [1,*], Vladislav V. Minaychev [1,2], Polina V. Smirnova [1], Margarita I. Kobiakova [1,2], Igor V. Smirnov [1], Roman S. Fadeev [2], Alexey A. Egorov [1], Artem A. Ashmarin [1], Kira V. Pyatina [2], Anatoliy S. Senotov [2], Irina S. Fadeeva [1,2,*] and Vladimir S. Komlev [1,*]

[1] A.A. Baikov Institute of Metallurgy and Materials Science, Russian Academy of Sciences, Leninskiy Prospect 49, Moscow 119334, Russia; vminaychev@gmail.com (V.V.M.); smirnova-imet@mail.ru (P.V.S.); ritaaaaa49@gmail.com (M.I.K.); baldyriz@gmail.com (I.V.S.)

[2] Institute of Theoretical and Experimental Biophysics, Russian Academy of Sciences, Pushchino 142290, Russia; fadeevrs@gmail.com (R.S.F.); a.s.senotov@gmail.com (A.S.S.)

* Correspondence: teterina_imet@mail.ru (A.Y.T.); aurin.fad@gmail.com (I.S.F.); komlev@mail.ru (V.S.K.)

Abstract: The injectable hydrated calcium phosphate bone-like paste (hCPP) was developed with suitable rheological characteristics, enabling unhindered injection through standard 23G needles. In vitro assays showed the cytocompatibility of hCPP with mesenchymal embryonic C3H10T1/2 cell cultures. The hCPP was composed of aggregated micro-sized particles with sphere-like shapes and low crystallinity. The ability of hCPP particles to adsorb serum proteins (FBS) was investigated. The hCPP demonstrated high protein adsorption capacity, indicating its potential in various biomedical applications. The results of the in vivo assay upon subcutaneous injection in Wistar rats indicated nontoxicity and biocompatibility of experimental hCPP, as well as gradual resorption of hCPP, comparable to the period of bone regeneration. The data obtained are of great interest for the development of commercial highly effective osteoplastic materials for bone tissue regeneration and augmentation.

Keywords: biocompatible materials; calcium phosphates; hydrated pastes; bone tissue

Citation: Teterina, A.Y.; Minaychev, V.V.; Smirnova, P.V.; Kobiakova, M.I.; Smirnov, I.V.; Fadeev, R.S.; Egorov, A.A.; Ashmarin, A.A.; Pyatina, K.V.; Senotov, A.S.; et al. Injectable Hydrated Calcium Phosphate Bone-like Paste: Synthesis, In Vitro, and In Vivo Biocompatibility Assessment. *Technologies* **2023**, *11*, 77. https://doi.org/10.3390/technologies11030077

Academic Editors: Kazushi Enomoto, Go Matsuba, Bungo Ochiai, Tomoya Higashihara and Sathish K. Sukumaran

Received: 15 May 2023
Revised: 12 June 2023
Accepted: 13 June 2023
Published: 15 June 2023

1. Introduction

The fabrication of injectable biocompatible, resorbable, osteoconductive, and bioactive bone-repairing pastes or gels is of great interest for the effective treatment of bone tissue defects [1–4]. Considering the present level of surgical technology and difficulties faced by traditional scaffolds, biocompatible and bioactive hydrated pastes or hydrogels persist as the most promising substances for the regeneration of bone tissue. The injectable form provides a great advantage in orthopedic and dental surgery, as it can be delivered through a cannulated needle or catheter into the bone defect in a minimally invasive way. They can also enable a more uniform distribution of bioactive calcium phosphate molecules within the damaged area [5,6]. From a clinical point of view, these materials are very attractive as they can be used with less discomfort for the patient and maximum convenience for the surgeon, both as a minimally invasive fillers for the consolidation of bone fragments or sinus lift surgery techniques and for the optimal filling of irregularly shaped bone defects [7]. In addition, injectable pastes or gels for filling bone voids (fillers) are very popular and are used to fill bone voids in the skeletal system and provide the possibility of multiple minimally invasive additions of material without traumatic surgical manipulations, including long-term treatment after a vertebral fracture or resection of tumors and bone cysts. The injectable materials and bone void filler market's steady growth is attributed to the increasing prevalence of various bone diseases such as bone tumors, osteoporosis, and bone infections [8,9].

Injectable bone materials may be cementitious or hydrogel based [10–13]. Acrylate bone cement has a variety of applications in orthopedic surgery (e.g., kyphoplasty and

vertebroplasty), but it also has some disadvantages, such as high heat generation during polymerization and a lack of integration with bone tissue [14–16]. The exothermic reaction during cement hardening has an additional damaging effect on the surrounding bone tissue and impairs regeneration processes [17,18]. Injectable hydrogel materials were developed as alternatives to cements. These hydrogel materials mainly consist of calcium phosphate powder evenly distributed in a polymer gel carrier. Calcium phosphates (CP) have been widely used as an injectable form of bone graft for orthopedic surgery owing to their excellent properties in terms of biocompatibility and osteoconductivity [1,19]. Such injectable CP gels are prepared from powders and liquid components that form a paste that can be injected into a bone defect in situ upon mixing [9]. In modern practice, injectable CPs are synthesized using a combination of rapidly and slightly resorbable calcium phosphates, such as calcium sulfate and hydroxyapatite in a resorbable polymer gel [10,12,13,20].

Bone is considered to be a hierarchical biocomposite primarily composed of hydroxyapatite bio-ceramic. Synthetic hydroxyapatite (HA) is widely used in medical applications because of its bio-inspired nature, lack of immunocompatibility, relatively low cost of production, and biological activity; HA is usually used as a slowly resorbable base [21]. Calcium sulfate has a nonporous crystalline structure and structure-independent rate of incorporation, which is consistent in relation to dissolution/incorporation [10,11]. Calcium sulfate (CaS) is typically used as a rapidly resorbable bioactive agent and as a regenerative material to repair bone defects because it releases calcium ions into the surrounding microenvironment and promotes osteoblast differentiation [10,11]. Hydrogels are strongly hydrated materials composed of three-dimensional hydrophilic polymeric systems comparable to those in normal tissues. The astuteness and rheological properties of hydrogels depend on the cross-linking between the polymer chains. Hydrogels were investigated as injectable materials because of their high tissue-like water content, ability to mimic the extracellular matrix, efficient mass transfer, instability to chemical and physical modifications, and minimally invasive delivery [22]. Injectable hydrogel cements mainly incorporate polymers, such as alginate, chitin, chitosan, cellulose, gelatin, and collagen, and synthetic polymers, such as polyethylene glycol (PEG), poly (lactic-co-glycolic acid) (PLGA), polycaprolactone (PCL), and poly (L-lactic acid) (PLLA) [23–26]. However, most CaP-polymer systems have many disadvantages such as an increased inflammatory reaction, which may be explained by the well-known adjuvant and immunoactivating properties of these substances [27–31]. Consequently, the inflammatory process may be more pronounced in such materials, and the rate of material-associated bone tissue regeneration may be significantly higher than that in the control group.

On the other hand, it is known that the most clinically effective pastes are based on the combination of nanosized HA with water. Clinical and animal data for the first generation of nanoscale calcium phosphate paste products (including NANOSTIM (Medtronic, Minneapolis, MN, USA) and ReproBone®novo (Ceramisys Ltd., Sheffield, UK)) are encouraging, suggesting that they are capable of promoting bone tissue regeneration [2,32]. Good clinical performance may be explained by an extremely high surface-area-to-volume ratio, bioinspired use of nanoscale calcium phosphates, and hydration layer on nanoparticle surfaces, which have a great influence on the subsequent protein adsorption and cell adhesion [33,34]. Meanwhile, CPs obtained by high-temperature synthesis do not have the necessary biological properties, and the body's response to them is limited to either the formation of a fibrous capsule around the material or the development of an inflammatory response [35–37].

We believe that injectable bone-repairing pastes must mimic the inorganic bone composition and have very specific hydrated surface kinetics to facilitate the migration, attachment, and proliferation of osteoprogenitor cells. Simultaneously, the calcium phosphate components used must be obtained under conditions as close as possible to physiological conditions, such as those occurring in native bone tissue.

Thus, the main goal of this study is to develop an approach for creating low-temperature injectable bone-like pastes, which are a combination of hydrated low-temperature hydroxyapatite with varying degrees of the crystalline phase.

2. Materials and Methods

2.1. Synthesis Procedure and Characterization

2.1.1. Synthesis of hCPP

The initial materials from Sigma Ltd. (St. Louis, MO, USA) were used in this work except for cases mentioned explicitly in the text. Distilled water and ethyl alcohol rectified from food raw materials were used for the synthesis and washing of filtration products.

The preparation of hydrated calcium phosphate paste (hCPP) samples was carried out by synthesizing HA powders. The liquid-phase method of deposition from solutions allows the receipt of non-stoichiometric HA with a low degree of crystallization and various shapes and with high specific surface area.

The hCPPs were prepared by stepwise mixing of ammonium phosphate salts with a concentration of 0.6 M and calcium nitrate with a concentration of 1 M under constant stirring with an overhead stirrer at 150–200 rpm. The pH value of the system in the range from 10.5 to 11.0 was maintained with an aqueous ammonia solution. The temperature of the reaction medium was maintained at 18 °C.

2.1.2. X-ray Diffraction Analysis

The phase compositions of the obtained hCPPs were studied on a Shimadzu XRD-6000 diffractometer with an automated imaging system allowing data collection, graphical processing, and identification of the obtained phases from the JCPDS 2003 data bank. X-ray phase studies for general phase analysis were performed on powder-dried samples under CuKα monochromatized radiation.

hCPPs were dried in a thermostat at 37 °C for 24 h. Then the dried hCPP powders were rubbed through a sieve with a 100 microns mesh size and transferred for analysis.

To confirm the reaction and the phase composition of the obtained powder, a sample of the obtained hCPP was also subjected to high-temperature treatment. For this purpose, a sample of 5–6 g was taken from the obtained hCPP samples, it was dried in a desiccator at 120 °C and then burned in a furnace with SiC heaters in an air atmosphere at 1250 °C for 2 h with 10 °C per minute heating rate.

The mass fraction samples were calculated using the normalized Chung method [38]. For this purpose, a full-profile analysis of the diffraction pattern was performed using the Jana 2006 software (wRp = 1.89%). The intensities of non-overlapping main peaks and the corundum numbers phases, specified in the cards of the JCPDS 2003 data bank, were used.

2.1.3. Infrared Spectroscopy

Infrared determination of absorption spectra of hCPP samples was carried out on a Nicolet Avatar 330 FT-IR spectrometer in the range of 4000–350 cm^{-1} with a resolution of 0.9 cm^{-1}. hCPP samples dried at 37 °C and hCPP powders after burning at 1250 °C were used for spectral analysis. For this study, samples of hCPP in powder form were mixed with potassium bromide. The spectra were analyzed based on reference and literature data.

2.1.4. Specific Surface Area hCPP

The specific surface area of calcium phosphate particles in the obtained hCPP was determined by BET low-temperature nitrogen adsorption on a Tristar 3000 Micromeritics instrument. This method measures the amount of substance required for the formation of an adsorption layer on the surface of a solid state. The specific surface area is computed from the number of molecules in the monolayer and the area occupied by each of them.

2.1.5. Dynamic Light Scattering (DLS) and ζ Potential

The particle size of hCPP samples was examined using a Zetasizer Nano ZS Pro Ultra analyzer (Malvern Panalytical Ltd., Malvern, UK) at 22 °C. The instrument settings were optimized automatically using the Zetasizer Software 7.13 (Malvern Panalytical Ltd., Malvern, UK). The average values were taken from three readings and all measurements were performed five times. For the ζ-potential study, dilution of the hCPP samples was performed with deionized water (Milli Q Advantage, Millipore, Burlington, MA, USA).

2.2. In Vitro Studies

2.2.1. Cell Culture

Murine embryonic mesenchymal cell line C3H/10T1/2 was obtained from ATCC (Manassas, VA, USA). Cells were grown in Basal Medium Eagle (Sigma-Aldrich, Milwaukee, WI, USA) supplemented with heat-inactivated fetal bovine serum (Gibco, Waltham, MA, USA) to a final concentration of 10% and 2 mM L-glutamine (Sigma-Aldrich, St. Louis, MO, USA), 40 µg/mL gentamicin sulfate (Sigma-Aldrich, St. Louis, MO, USA), under conditions of 5% CO_2 content in the air and at 37 °C. Cells of 7–10 passages were used in the experiments. The cell cultures were tested for mycoplasma infection using the MycoFluor™ Mycoplasma Detection Kit (Thermo Fisher Scientific, Waltham, MA, USA), and no mycoplasma was detected.

2.2.2. Cytotoxicity Assays

Murine embryonic mesenchymal cell line C3H/10T1/2 was seeded in 5×10^3 cells in 100 µL of complete growth medium into 96-well plates (Corning Inc., Corning, NY, USA). After 24 h of cultivation, the medium was replaced with 100 µL of medium containing hCPP, at concentrations of 10, 3, 1, 0.3, and 0.1 mg/mL, and the cultivation was continued for 24 and 96 h. The cells in the control conditions were cultivated in the medium without the addition of hCPP. hCPP was presterilized with 75% ethanol according to the indicated method [39]. Then, cell viability was analyzed, as well as morphological analysis of the cell culture conditions.

The cytotoxicity of hCPP and the morphological state of the cell culture were analyzed by in vitro staining of cells with the fluorescent dyes Hoechst 33342 (stains nuclei of living and dead cells blue), propidium iodide (stains nuclei of dead cells red), and calcein AM (stains cytoplasm of living cells green). Cells were stained by adding 1 µg/mL Hoechst 33342 (Sigma-Aldrich, St. Louis, MO, USA), 1 µg/mL propidium iodide (PI) (Sigma-Aldrich, St. Louis, MO, USA), and 2 mM Calcein AM (Sigma-Aldrich, St. Louis, MO, USA) to the culture medium. The staining was performed in a CO_2 incubator for 30 min at 37 °C and 5% CO_2 in the air.

Microscopic analysis of the stained cell cultures and micro images were made on a Nikon Eclipse Ti-E (Nikon, Tokyo, Japan). The plate with cells and examined samples was transferred to a microscope chamber at 37 °C and 5% CO_2 content. Cytotoxicity was analyzed by calculating the number of live and dead cells per field of view using the ImageJ software (https://imagej.nih.gov/ij/ (accessed on 19 April 2022)).

2.2.3. Protein Adsorption Assay

To determine the protein sorption capacity, hCPP was incubated in PBS with 10% FBS for 24 h. The final concentration of hCPP in the mixture was 10 mg/mL. PBS with 10% FBS was used as a control. The samples were incubated on an orbital shaker (S-3M A10, ELMI, Riga, Latvia) at a temperature of 37 °C with constant stirring at 21 rpm. To remove hCPP after incubation, the samples were subjected to centrifugation for 5 min at 5000 rpm using a Universal 320R centrifuge (Hettich, Westphalia, Germany). Protein concentration in the supernatant was determined using the Bradford method [40] at an absorption wavelength of 595 nm using an Imark plate reader (Bio-Rad, Hercules, CA, USA).

2.3. In Vivo Studies

2.3.1. Animals

Twenty Wistar male rats, weighing 190–200 g (age two months), were used. Animals were individually housed in a temperature-controlled room (22 °C) and fed a standard diet, with full access to water and food. The experiments were carried out according to the Regulations for Studies with Experimental Animals (Decree of the Russian Ministry of Health of 12 August 1997, No. 755). The protocol was approved by the Commission on Biological Safety and Ethics at the Institute of Theoretical and Experimental Biophysics, Russian Academy of Sciences (March 2022, protocol N26/2022). For the experiments, rats were divided into four groups (five in each group) and independent replicates were conducted for each group.

2.3.2. Surgical Subcutaneous Injection

The model of ectopic (subcutaneous) implantation of biomaterials was used to study the biocompatibility of hCPP samples in vivo (ISO 10993-6). This model is advantageous and in addition to biocompatibility and safety analysis, it is used to evaluate the osteoinductive and osteogenic effects of substances [41,42]. Therefore, a heterotopic implantation model (under the skin, into the muscle, etc., but not into the bone) is the most reliable for revealing the osteoinductive and osteogenic potential of the materials under development.

The manipulations were performed under general anesthesia with Xylazine 13 mg/kg (Interchemie, Castenray, The Netherlands) and Zoletil 7 mg/kg (Virbac, Carros, France). An aliquot of paste (500 mL) or saline solution was subcutaneously injected into the dorsal interscapular area of each group of animals. For post-surgical recovery, the animals were exposed to a heating plate until awakening. The animals from each group were randomly divided to be euthanized (carbon dioxide protocol) after 3, 8, or 13 weeks of the subcutaneous injection. Immediately after humane euthanasia, to prevent autolysis, and instantly after the withdrawal, the samples of implanted materials, with surrounding tissues of the recipient bed, were washed for 30 s with a cold (14 °C) isotonic solution and fixed for 48 h in neutral buffered formalin (NBF) at the tissue–volume fixator volume ratio 1:30.

2.3.3. Histological Analysis

The hCPP samples were explanted with surrounding tissue and assessed, as described below, for the subsequent morphological study. Immediately after humane euthanasia, to prevent autolysis instantly after the withdrawal, samples of implanted materials, with surrounding tissues of the recipient bed, were washed for 30 s with a cold (14 °C) isotonic solution and fixed for 48 h in 10% neutral buffered formalin (NBF) at the tissue–volume fixator volume ratio 1:30. For the morphological study, after fixation samples were dehydrated and paraffin embedded, sections (with a thickness of 4 μm) were prepared and stained using H&E (Mayer's Hematoxylin and Eosin Y) and differential staining for calcium deposits alizarin red S (by the McGee-Russell method) and collagen/non collagen structures (by Lillie's trichrome method) [43]. The micrographs of the stained histological samples were obtained on a Nikon Eclipse Ti-E microscope station (Nikon, Tokyo, Japan) and processed using the software NIS Elements AR4.13.05 (Build 933). The maturity of neocollagenous connective tissues around the samples was evaluated with its thickness and a relative area of blood vessels. The high maturity corresponded to minimal inflammation in the low-thickness tissues with a small number of vessels.

2.4. Statistical Analysis

Results are presented as the mean ± standard deviation (M ± SD). Each of the in vitro experiments was carried out at least four times ($n \geq 4$). The statistical significance of the difference was determined using Mann–Whitney U test. The size of the observed effects was assessed using standardized mean difference (Hedges's g).

The design of the experiment and related statistics (U test) were carried out using Python 3 (ver. 3.10.10) in development environment Spyder (v. 5.4.1) with libraries Pandas (v. 1.5.2), Numpy (v.1.24.2), and Scipy (v. 1.10.0). Plots were created using Python 3 (ver. 3.10.10) with libraries Seaborn (v. 0.12.2) and Matplotlib (v. 3.7.0).

3. Results

3.1. Results of Structural and Physical–Chemical Analyses

The hCPPs were obtained by liquid-phase synthesis of HA by precipitation from solution without subsequent thermal treatment. The synthesis product was a white paste consisting of a fine powder. The results of measurements of the specific surface area of the powders were 80 ± 0.5 m^2/g with the particle size calculated from the specific surface area of hCPP powders being in the range of 25–30 nm. However, the determination of the size of calcium phosphate particles in the region of small sizes is less reliable than the parameter of the coherent scattering region.

Figure 1 shows the IR spectra of both compounds. The precipitate before sintering (Sample-0) has a weak absorption band of the OH- group at 3575 cm^{-1}, indicating low crystallinity of the HA powder. The spectral region from 900 to 1100 cm^{-1} characterizes the symmetric and asymmetric vibrations of the PO_4^{3-} group. The peaks at 564 and 603 cm^{-1} belong to the P-O deformational vibrations ($\nu 4$). The mode at 875 cm^{-1} may belong to both HPO_4^{3-} and CO_3^{2-} groups [44]. The vibrations modes of the CO_3^{2-} group are also detected at 1415 and 1458 cm^{-1}. The peak at 1649 cm^{-1} indicates the presence of adsorbed water. These data are in good agreement with previous studies [45,46].

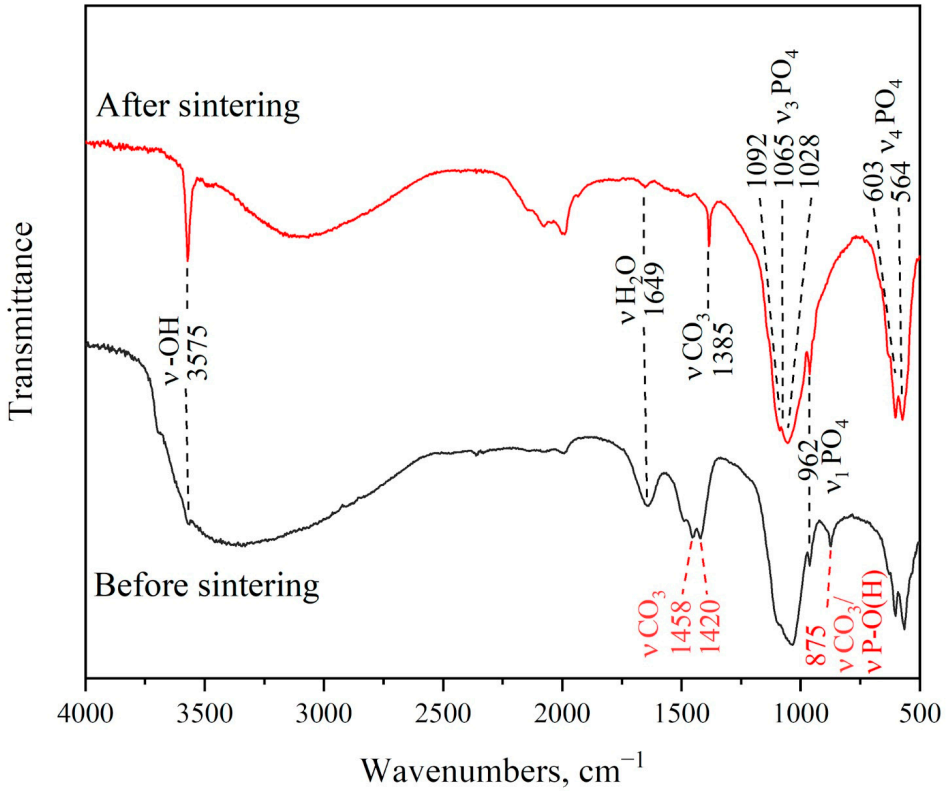

Figure 1. Fourier infrared spectra of hCPP samples after synthesis and firing at 1250 °C.

After sintering, a sharp peak of the OH- group appears at 3566 cm^{-1}, indicating an increase in the crystallinity of the samples and the presence of the HA phase. The peaks of the phosphate groups at 960–1100 cm^{-1} and 550–620 cm^{-1} remain unchanged. The mode of the hydrophosphate group at 875 cm^{-1} decreases. The modes belonging to CO_3^{2-} and adsorbed water also decrease.

The results of the X-ray diffraction (XRD) analysis are presented in Figure 2. Before sintering (Sample-0), the precipitate was amorphous (or with small crystallite size), which causes the FWHM of adjacent peaks to overlap. This leads to difficulties in determining the phase composition and indexing of the diffraction pattern. Some observed maxima on the XRD pattern constitute a superposition of several peaks. Their indices were compared with card №84-1998 of the XRD base ICDD (Powder Diffraction File, Alphabetical Index Inorganic Compounds, Pensylvania: JCPDS, 1997) and are presented in Table 1. The peaks that are not a superposition of the other two peaks are shifted slightly to the right relative to the card, due to the fact that the diffractogram was taken without a monochromator; that is, the Kα2 shoulder appears at the far angles of 2θ and the peak becomes wider than it is. This could lead to inaccurate determination of the lattice parameters of the samples. After sintering, the crystallinity of the samples increased, allowing us to identify two phases: HA, corresponding to card №84-1998, and α-TCP, corresponding to card number 29-359. The indices of the reflections of both phases are also presented in Table 1.

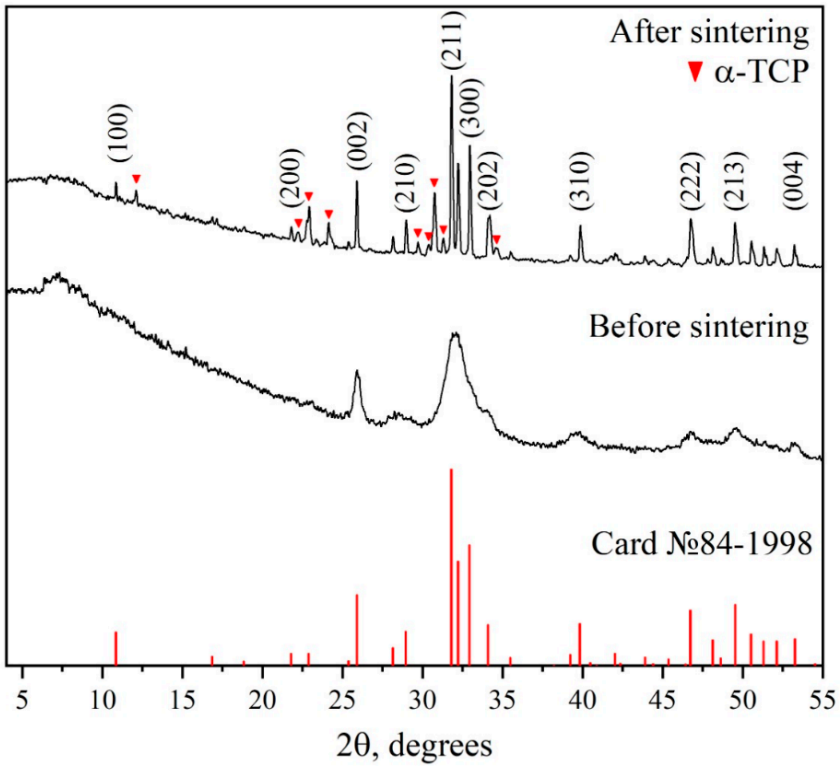

Figure 2. XRD data of hCPP samples upon synthesis after firing at 1250 °C.

The mass ratios in the final product were calculated by the Chung method (corundum numbers). Samples after sintering contain about 44 ± 2% of the α-TCP phase. The α-TCP phase is not visible in the IR spectrum because the phosphate groups have the same vibration frequencies as in HA [47]. According to the fact that the HPO_4^{3-} group (mode at 875 cm^{-1}) was present before annealing, we suggested that initially two phases precipitated from the solution: hydroxyapatite $Ca_{10}(PO_4)_6(OH)_2$ and calcium-deficient hydroxyapatite (CDHAp) $Ca_9(HPO_4)(PO_4)_5(OH)$. The diffraction pattern of CDHAp is presented in card number №46-905. This phase has the same crystal symmetry, space group, and lattice parameters as HA, so it produces reflections that are almost identical to pure HA. However, due to the low crystallinity of our samples, it is not possible to distinguish the phase composition of the precipitate. CDHAp has reflexes with the same Miller indices and at very close angles of two theta as the HA card. Only the intensity differs, but not significantly.

Upon heating, CDHAp decomposes into α-TCP and water, according to the mechanism described by Y. Li and et al. [48]:

$$Ca_9(HPO_4)(PO_4)_5(OH) \rightarrow 3Ca_3(PO_4)_2 + H_2O;$$

Table 1. List of the Peaks Observed in the X-Ray Powder Diffraction Pattern.

Sample-0		HA (1250 °C)		HA (1250 °C)		α-TCP	
2Theta	**(hkl)**	**2Theta**	**(hkl)**	**2Theta**	**(hkl)**	**2Theta**	**(hkl)**
		10.86	100	55.98	322	12.11	031
		21.81	200	57.21	313	22.23	201
		22.93	111	58.31	204	22.77	–162
		25.39	201	58.88	330	23.38	–204
25.96	002	25.91	002	60.03	420	23.87	033
28.49	102, 210	28.16	102	60.49	331	24.14	–261
		28.99	210	61.76	421	24.31	043
32.07	211, 112	31.83	211	63.10	502	26.72	–334
		32.24	112	63.53	510	29.73	–361
33.40	300, 202	32.97	300	64.14	304	30.38	–191
		34.17	202	65.18	511	30.76	034
		35.53	301	66.51	422	31.30	–335
39.67	212, 310	39.24	212			34.62	400
		39.88	310			41.43	
		40.48	221			41.76	
		40.87	103				
		42.07	311				
		42.33	302				
		43.90	113				
		44.40	400				
		45.40	203				
46.83	222	46.79	222				
		48.16	312				
		48.71	320				
49.67	213	49.56	213				
		50.59	321				
51.51	410	51.37	410				
		52.17	402				
53.26	004	53.26	004				

Y. Li and co-workers also worked with a biphasic ceramic consisting of α-TCP and HA [49]. The spectra of their intermediate phase are similar to the spectra presented here. The CO_3^{2-} absorption bands at 1415 and 1458 cm^{-1} are also present in the unheated ceramic, but after sintering they merge into a single peak at 1385 cm^{-1}. The authors suggest that the bands at 1415 and 1458 cm^{-1} are characteristic of CO_3^{2-} groups incorporated into the structure of CDHAp [50]. Upon sintering, the CO_3^{2-} group is incorporated into the HA structure, which leads to a slight decrease in lattice parameters (Table 2) [44].

Table 2. The cell dimensions of the natural HA and precipitates formed.

Sample	a(Å)	c(Å)	V(Å3)
Card №84-1998	9.4166	6.8745	527.9
Sample_0	9.39(4)	6.875(12)	525.3(22)
HA	9.4062(18)	6.8707(15)	526.45(15)

3.2. Results of Dynamic Light Scattering (DLS) and ζ-Potential Assay

The results of DLS (A) and ζ-potential (B) are presented in Figure 3. As can be seen from the presented data, hCPP was identified as a unimodal narrow-peak dispersed system,

with an average particle size of 1416 ± 174.8 nm. Figure 3C presents the data on the high injection capacity of hCPP. The resulting paste-like material easily penetrated through the 23G needle of a standard syringe for subcutaneous and intramuscular injections.

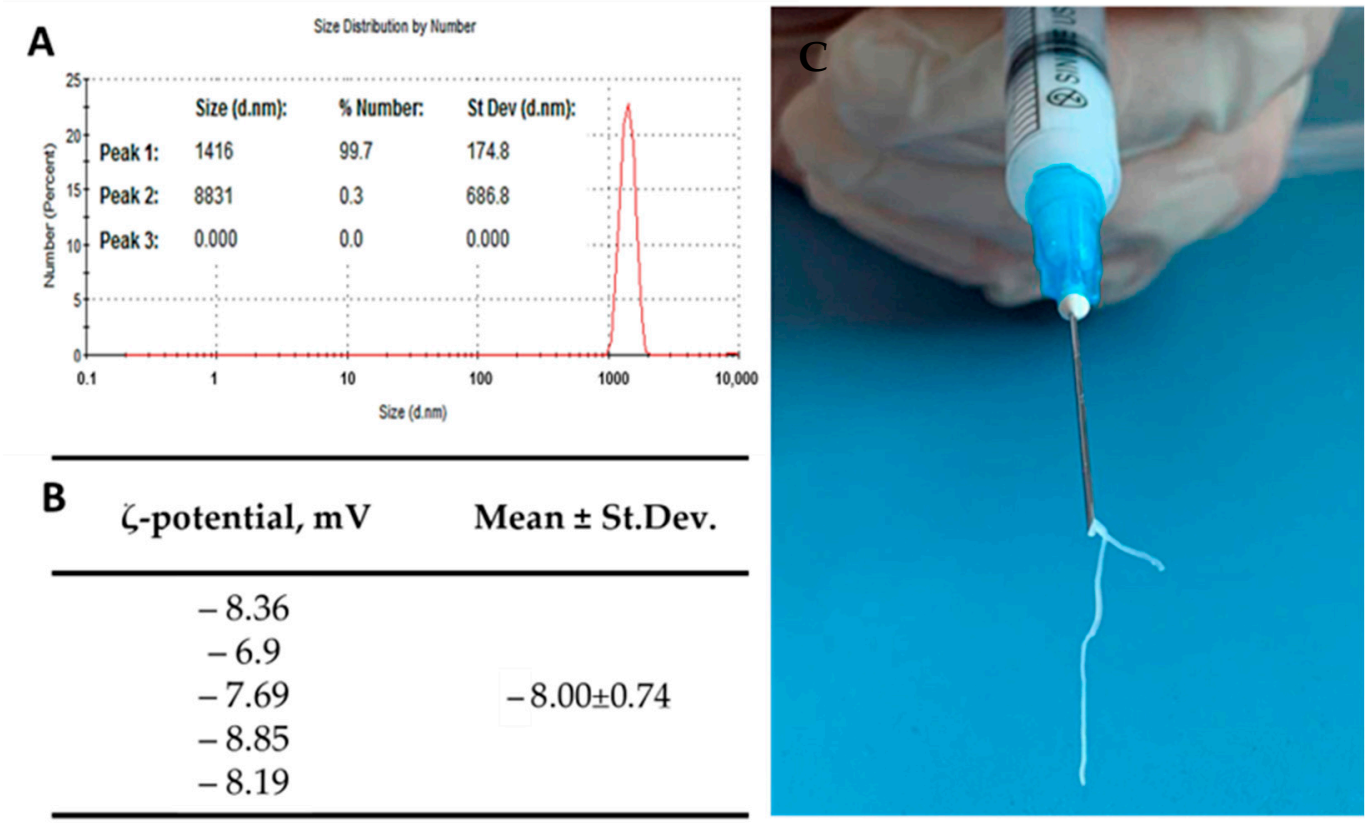

Figure 3. Results of DLS (**A**), ζ-potential (**B**), and injection capacity of the resulting hydrated calcium phosphate paste (**C**).

3.3. Results of Cytotoxicity Assays

The results of dose-dependent cytotoxicity of the paste-like material are shown in Figure 4. Complete cell death after cultivation with hCPP particles for 24 h was observed only at concentrations of 3 mg/mL or higher. After the first day of cultivation, the number of living cells comparable to the control was observed at a concentration of 0.1 mg/mL (93.60 ± 4.04%). After 96 h of cultivation with hCPP samples, all cells were observed to die at maximum concentrations of 3 mg/mL and 10 mg/mL (Figure 4A). At the same time, at standard concentrations of 1.0 and 0.3 mg/mL, a greater number of living cells were observed after 96 h of cultivation, compared with 24 h of cultivation, which indicated the proliferative activity of the cells (Figure 4B). Thus, at a concentration of 1 mg/mL after 96 h of cultivation, the percentage of living cells increased to 70.67 ± 6.02, and at a concentration of 0.3 mg/mL, the value was comparable to that of the control (92.70 ± 2.52).

Such dose-dependent cytotoxic properties of the material under in vitro conditions may be associated with the presence of an amorphous phase. Since the amorphous phase is characterized by greater solubility than the crystalline one [51], there is a possibility of cytotoxic Ca^{2+} ions being released at the cell–material interface due to the acidification of the environment by cells. At the same time, high cell survival in the presence of the studied materials at standard operating concentrations (1.0 mg/mL) and the signs of proliferative activity in the seeded cells indicate the cytocompatibility of the obtained materials. In turn, the presence of an amorphous phase (and free Ca^{2+} ions) in the microenvironment of the material under in vivo conditions should have a differentiating effect on progenitor cells during hCPP implantation in the bone environment.

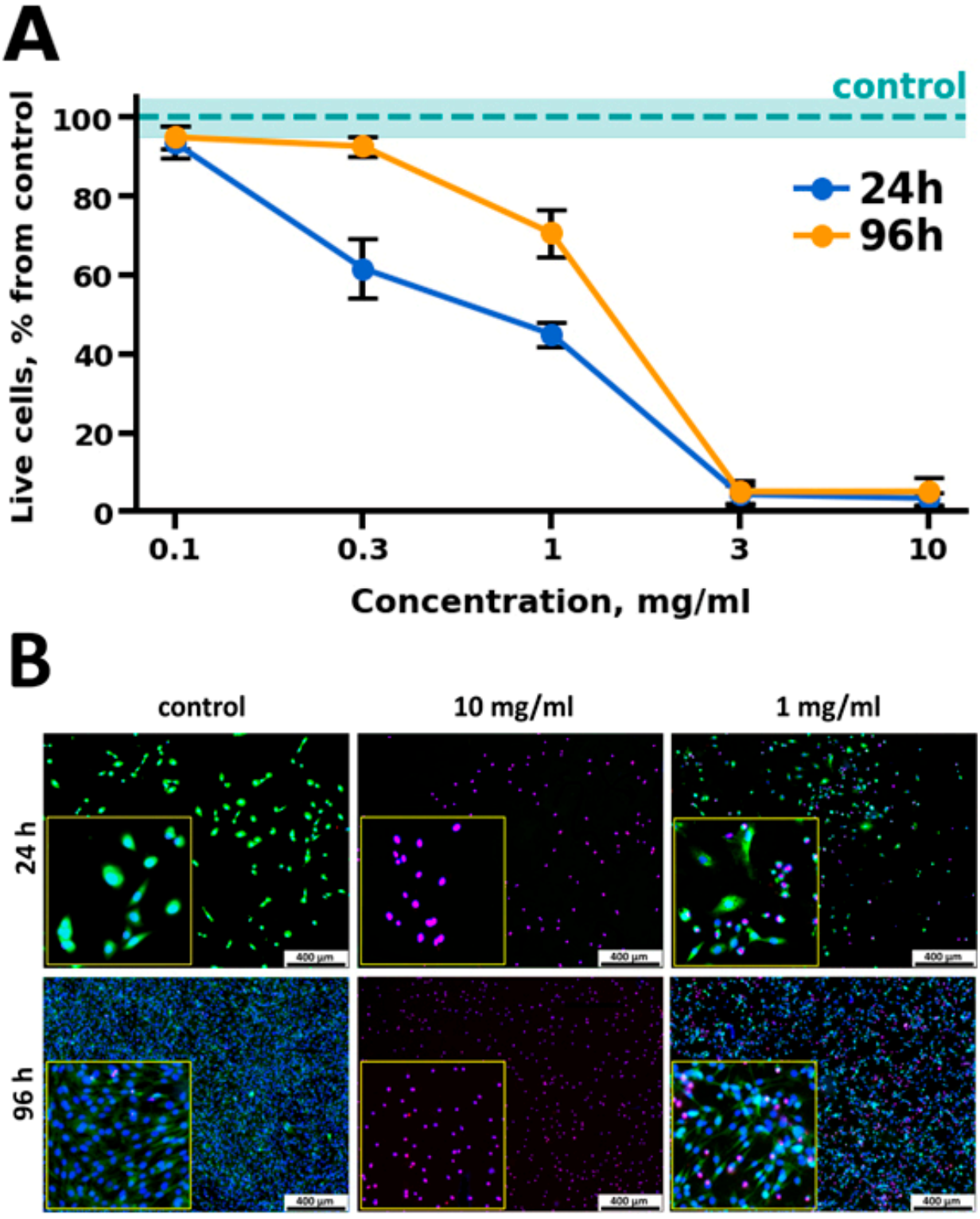

Figure 4. Results of cytotoxic effects of hCPP cultured with murine embryonic mesenchymal cell line C3H/10T1/2 at concentrations of 0.1, 0.3, 1.0, 3.0, and 10.0 mg/mL, after 24 h and 96 h of cultivation (**A**). Fluorescence microphotographs of cell line C3H/10T1/2 in the control and the presence of 10 mg/mL, 3 mg/mL, and 1 mg/mL hCPP (**B**): cell nuclei are stained with Hoechst 33342 (blue), the cytoplasm of live cells is stained with calcein AM (green), and nuclei of dead cells are stained with PI (purple).

3.4. Results of Protein Adsorption Assay

The first stage of the interaction of a biomaterial with the human body is the sorption of proteins from tissue fluid by its surface. At the same time, with respect to different particles, the key moment of this interaction is the formation of the protein corona surrounding the outer layer of particles [52]. It is believed that the emerging protein corona gives particles a new biological identity, as it changes both physicochemical characteristics and biological properties [53,54]. Therefore, it is important to evaluate the sorption capacity of hCPP. For this purpose, the material was cultured in PBS containing an equivalent amount of protein (10% FBS) in the culture medium for 24 h.

After cultivation of the hCPP with PBS with the addition of 10% FBS, a decrease from 2.1 ± 0.06 to 0.93 ± 0.06 mg/mL in the protein content in the incubation medium was observed (Figure 5).

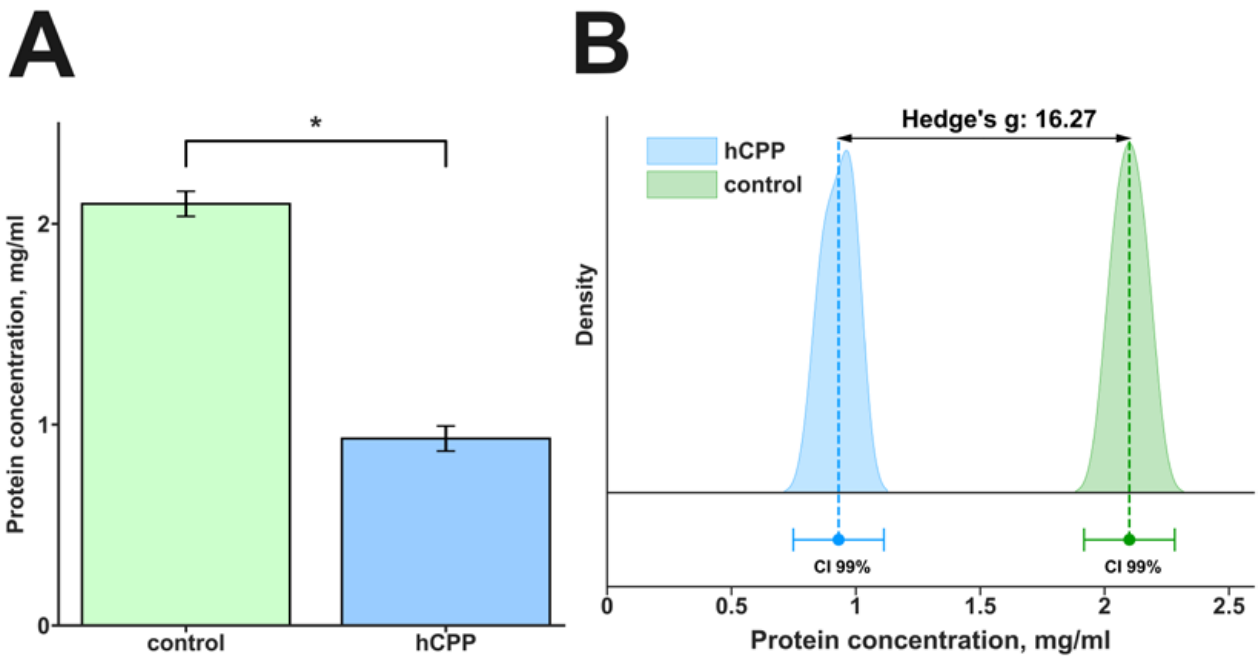

Figure 5. Results of protein adsorption of hCPP (10 mg/mL) cultured with PBS + 10% FBS (**A**). Effect size is shown using the standardized mean difference (Hedges's g). Hedges's coefficient $g \geq 0.80$ indicates a large effect (**B**). *—statistically significant difference compared to control, $p < 0.05$. CI—confidence interval.

These findings (especially the effect size Hedges's g, 16.27) represent the strong sorption capacity of hCPP in relation to proteins.

3.5. Results of In Vivo Biocompatibility Assays

Three weeks after subcutaneous injection of hCPP samples into rats, a neocollagen capsule was formed around the material (Figure 6C) without signs of cell death inside the fibers and fusion of collagen fibers into a dense scar-like fibrous capsule. The neocollagen capsule was saturated with mature microvessels (Figure 6C, black arrows), indicating positive perception of hCPP by the organism. The high maturity of the neocollagenous capsula with a small number of definitive vessels corresponded to minimal inflammation in the surrounding tissues. Simultaneously, the main layer of the material was preserved and represented a sufficiently hydrated calcium phosphate-protein substrate. Inside the capsule, crushing of a solid layer of material by migrating cells into spheres of smaller diameter (Figure 6D) and their gradual resorption were observed. Resorption of hCPP was performed from the periphery to the center. There were no signs of acute inflammation or signs of material-associated osteogenesis for 3 weeks.

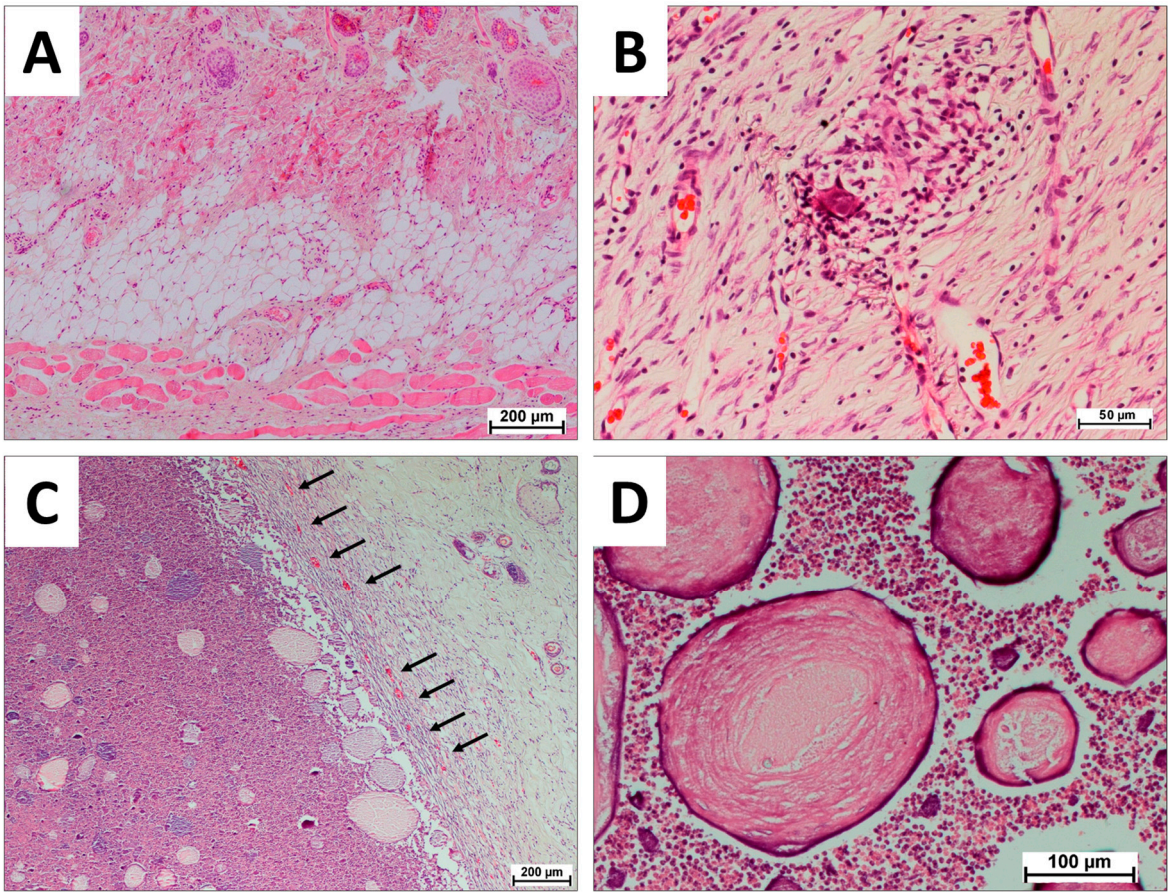

Figure 6. Histological analysis of injected hCPP samples in the control (**A**,**B**) and experimental (**C**,**D**) groups after three weeks of implantation. Hematoxylin and eosin staining (H&E, cell nuclei colored blue, erythrocytes colored red, and muscle tissue colored pink; black arrows—mature microvessels in neocollagen capsule); light microscopy. Explanations in the text.

No signs of inflammation or differences from healthy surrounding tissues were observed in the control animals that received an injection of saline solution (Figure 6A,B). After 6 and 13 weeks after injection, the tissues around the injection of the solution were indistinguishable from healthy tissues, because of which the histology of these tissues was not further considered.

Six weeks after subcutaneous implantation, separation of the capsule material from the hCPP and an increase in the penetration zone of the cells into the material were observed. The hCPP material lost its hydration at this time and cracked (Figure 7A,B), forming a relatively loose calcium phosphate-protein substrate with a large number of cells (Figure 7B, yellow arrows). The capsule around the material was partially calcined, while the calcium deposits were small in size and captured the newly formed collagen tissue around the foci of the hCPP material (Figure 7C). The resorption of hCPP during this observation period averaged at 25%.

Thirteen weeks after subcutaneous injection of hCPP, separation of the material and capsule was observed with pronounced signs of cellular mineralization, which indicated the osteogenic nature of the capsule involution (Figure 7H). At the same time, as well as for a period of six weeks, hCPP material was cracking (Figure 7E–G) and a relatively loose calcium phosphate-protein substrate with a large number of cells was observed. The resorption of hCPP material during this observation period averaged at 60%. During this observation period, a distinctive feature of hCPP material was the formation of a mature collagen matrix around small fragments of hCPP, resembling a spongy extracellular matrix (Figure 7E, green arrows; Figure 7G, neocollagen matrix colored turquoise).

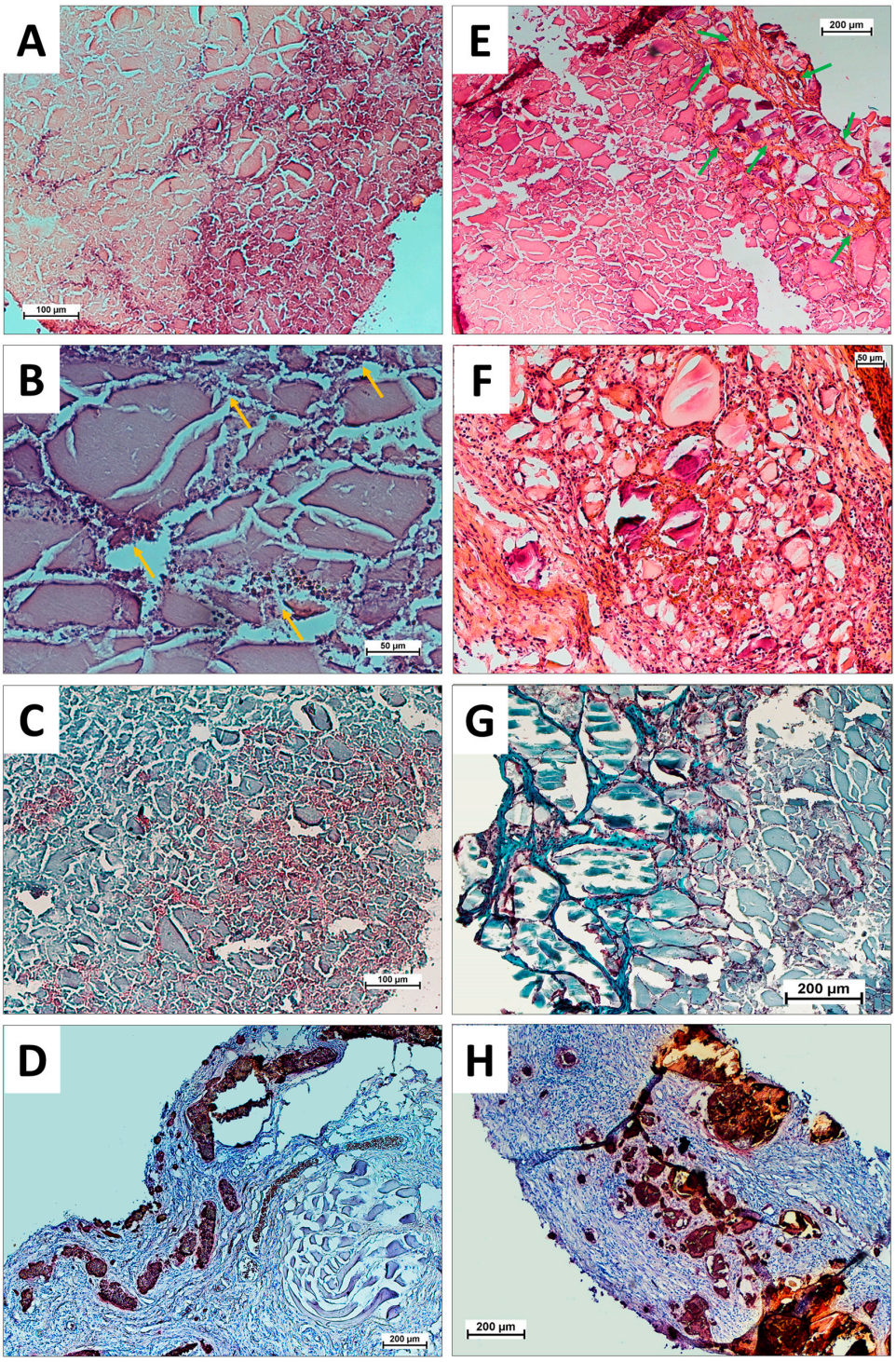

Figure 7. Histological analysis of injected hCPP samples after six (**A**–**D**) and thirteen (**E**–**G**) weeks. (**A**,**B**,**E**,**F**) Hematoxylin and eosin staining (H&E, cell nuclei colored blue, erythrocytes colored red, and muscle tissue colored pink; yellow arrows—cells migrated into the cracked calcium phosphate-protein substrate; green arrows—neocollagen trabecula-like matrix); (**C**,**G**) Masson–Goldner staining (cell nuclei colored purpuric, neocollagen matrix colored turquoise, calcium-protein deposits colored pale blue); (**D**,**H**) alizarin red S staining (calcium deposits colored orange-red, cell nuclei colored dark blue); light microscopy. Explanations in the text.

The results indicated the nontoxicity, biocompatibility, and osteoconductivity of the experimental hCPP, as well as the gradual resorption of hCPP, which was comparable

to the period of bone regeneration. Thus, the results obtained by us in this study of injectable hydrated calcium phosphate bone-like paste represent a step towards a new class of minimally invasive, osteoconductive, injectable bone-like pastes with appropriate resorption rates, which are easy to produce and, depending on their physicochemical and biological characteristics, can be carriers of any additional biological activities, thus showing promise for clinical applications in regenerative engineering.

4. Conclusions

The hydrated calcium phosphate unimodal narrow-peak dispersed system, with an average particle size of 1416 ± 174.8 nm and ζ-potential of 8 ± 0.74 mV, with strong sorption capacity (Hedges's g, 16.27) and an absence of toxic effects at standard concentrations of 1.0 and 0.3 mg/mL of hCPP was obtained in this work using the liquid-phase precipitation method from solution. It was found that at a concentration of 1 mg/mL after 96 h of cultivation, the percentage of living cells increased to 70.67 ± 6.02%, and at a concentration of 0.3 mg/mL, the value was comparable to that of the control (92.70 ± 2.52%). This biocompatibility study of hCPP implantation in animals showed that the injectable paste developed using our approach has a pronounced biocompatibility and a suitable resorption time. Our studies revealed that the hCPP obtained with a significant portion of the amorphous phase can initiate the formation of a trabecula-like neocollagen matrix after 13 weeks of implantation in the model of ectopic implantation in rats, which indicates an osteoinductive effect of the material obtained.

Thus, we can conclude that the resulting injectable hydrated calcium phosphate bone-like paste is easy to synthesize, efficiently adsorbs extracellular fluid protein, and provides a biocompatible basis for the creation of effective osteoplastic materials for minimally invasive treatment in maxillofacial surgery and traumatology. The pronounced adsorption ability of this paste is its undoubted advantage, since both in comparison with our own data and the data in the scientific literature, the adsorption of the most common extracellular protein (albumin) on the surface of particles can radically increase the osteogenic ability of materials [55,56]. In addition, the injectable ability of the resulting paste, coupled with its optimal dimensional characteristics and hydration of particles, is a significant advantage of this material for creating injectable pastes to fill bone voids in orthopedics. However, the insufficient osteogenic potential of the studied hCPP demonstrates that it can be successfully used for "fresh" bone trauma, but not in the case of "old" fibrotic trauma or nonunion, which requires materials with additional artificial osteoinductive activity. Growing geriatric populations prone to fractures and bone injuries are anticipated to increase the demand for products that treat these injuries in the coming years. Furthermore, the growing demand for eluting bone fillers (e.g., with antibiotics or growth factors) and the rising number of new product launches by market actors, are expected to boost market growth from the forecast period to 2030 [8,9].

Thus, the developed hCPP (under the conditions of further modification by selected osteoinductive agents) could be a suitable candidate as a safe bone-forming injectable material for bone tissue regeneration. This study is the first step toward the development of minimally invasive, osteoconductive, and injectable bone-like pastes with applicable resorption rates and low production costs.

Author Contributions: Conceptualization, I.S.F. and A.Y.T.; methodology, I.V.S. and V.V.M.; validation, R.S.F. and A.S.S.; formal analysis, A.A.A.; investigation, M.I.K., V.V.M. and K.V.P.; writing—original draft preparation, V.V.M., A.A.E., and P.V.S.; writing—review and editing, I.S.F., A.Y.T., and V.S.K.; visualization, I.V.S.; supervision, V.S.K. All authors have read and agreed to the published version of the manuscript.

Funding: This research was funded by the Russian Science Foundation (RSF, №21-73-20251).

Institutional Review Board Statement: The animal study protocol was approved by the Ethics Committee of the Institute of Theoretical and Experimental Biophysics of the Russian Academy of Sciences (protocol #26/2022 from 5 March 2022).

Informed Consent Statement: Informed consent was obtained from all subjects involved in this study.

Data Availability Statement: Data available upon request from the authors.

Acknowledgments: This work was carried out using the equipment of the Center for the Collective Use of Research Equipment at the ITEB RAS and IMET RAS.

Conflicts of Interest: The authors declare no conflict of interest.

References

1. Raucci, M.G.; D'Amora, U.; Ronca, A.; Ambrosio, L. Injectable Functional Biomaterials for Minimally Invasive Surgery. *Adv. Healthc. Mater.* **2020**, *9*, e2000349. [CrossRef] [PubMed]
2. Subbiah, R.; Lin, E.Y.; Athirasala, A.; Romanowicz, G.E.; Lin, A.S.P.; Califano, J.V.; Guldberg, R.E.; Bertassoni, L.E. Engineering of an Osteoinductive and Growth Factor-Free Injectable Bone-Like Microgel for Bone Regeneration. *Adv. Healthc. Mater.* **2023**, *12*, e2200976. [CrossRef]
3. Phogat, K.; Ghosh, S.B.; Bandyopadhyay-Ghosh, S. Recent advances on injectable nanocomposite hydrogels towards bone tissue rehabilitation. *J. Appl. Polym. Sci.* **2023**, *140*, e53362. [CrossRef]
4. Harrison, C.J.; Hatton, P.V.; Gentile, P.; Miller, C.A. Nanoscale Strontium-Substituted Hydroxyapatite Pastes and Gels for Bone Tissue Regeneration. *Nanomaterials* **2021**, *11*, 1611. [CrossRef]
5. Zeimaran, E.; Pourshahrestani, S.; Fathi, A.; Razak, N.A.B.A.; Kadri, N.A.; Sheikhi, A.; Baino, F. Advances in bioactive glass-containing injectable hydrogel biomaterials for tissue regeneration. *Acta Biomater.* **2021**, *136*, 1–36. [CrossRef]
6. Hao, J.; Chou, J.; Kuroda, S.; Otsuka, M.; Kasugai, S.; Lang, N.P. Strontium hydroxyapatite in situ gel-forming system—A new approach for minimally invasive bone augmentation. *Clin. Oral Implant. Res.* **2015**, *26*, 581–585. [CrossRef] [PubMed]
7. Qu, Y.; Zhuang, H.; Zhang, M.; Wang, Y.; Zhai, D.; Ma, B.; Wang, X.; Qin, C.; Huan, Z.; Wu, C. Bone cements for therapy and regeneration for minimally invasive treatment of neoplastic bone defects. *J. Mater. Chem. B* **2021**, *9*, 4355–4364. [CrossRef] [PubMed]
8. Fortune Business Insights. Available online: https://www.researchandmarkets.com/reports/5206327/bone-grafts-and-substitutes-market-by-type (accessed on 1 May 2023).
9. The Global Bone Void Fillers Market. Available online: https://www.fortunebusinessinsights.com/industry-reports/bone-void-fillers-market-101015 (accessed on 1 May 2023).
10. O'Neill, R.; McCarthy, H.O.; Montufar, E.B.; Ginebra, M.P.; Wilson, D.I.; Lennon, A.; Dunne, N. Critical review: Injectability of calcium phosphate pastes and cements. *Acta Biomater.* **2017**, *50*, 1–19. [CrossRef]
11. Xu, H.H.K.; Wang, P.; Wang, L.; Bao, C.; Chen, Q.; Weir, M.D.; Chow, L.C.; Zhao, L.; Zhou, X.; Reynolds, M.A. Calcium phosphate cements for bone engineering and their biological properties. *Bone Res.* **2017**, *5*, 17056. [CrossRef]
12. Yasmeen, S.; Lo, M.K.; Bajracharya, S.; Roldo, M. Injectable scaffolds for bone regeneration. *Langmuir* **2014**, *30*, 12977–12985. [CrossRef]
13. Bai, X.; Gao, M.; Syed, S.; Zhuang, J.; Xu, X.; Zhang, X.Q. Bioactive hydrogels for bone regeneration. *Bioact. Mater.* **2018**, *3*, 401–417. [CrossRef] [PubMed]
14. Fang, C.-H.; Lin, Y.-W.; Sun, J.-S.; Lin, F.-H. The chitosan/tri-calcium phosphate bio-composite bone cement promotes better osteo-integration: An in vitro and in vivo study. *J. Orthop. Surg. Res.* **2019**, *14*, 162. [CrossRef] [PubMed]
15. Khandaker, M.; Meng, Z. The Effect of Nanoparticles and Alternative Monomer on the Exothermic Temperature of PMMA Bone Cement. *Procedia Eng.* **2015**, *105*, 946–952. [CrossRef] [PubMed]
16. Khandaker, M.; Vaughan, M.B.; Morris, T.L.; White, J.J.; Meng, Z. Effect of additive particles on mechanical, thermal, and cell functioning properties of poly(methyl methacrylate) cement. *Int. J. Nanomed.* **2014**, *9*, 2699–2712. [CrossRef]
17. Jeong, J.; Kim, J.H.; Shim, J.H.; Hwang, N.S.; Heo, C.Y. Bioactive calcium phosphate materials and applications in bone regeneration. *Biomater. Res.* **2019**, *23*, 4. [CrossRef]
18. Alt, V.; Bechert, T.; Steinrücke, P.; Wagener, M.; Seidel, P.; Dingeldein, E.; Domann, E.; Schnettler, R. An in vitro assessment of the antibacterial properties and cytotoxicity of nanoparticulate silver bone cement. *Biomaterials* **2004**, *25*, 4383–4391. [CrossRef]
19. Lodoso-Torrecilla, I.; van den Beucken, J.J.J.P.; Jansen, J.A. Calcium phosphate cements: Optimization toward biodegradability. *Acta Biomater.* **2021**, *119*, 1–12. [CrossRef]
20. Liu, S.; Fu, H.; Lv, Y.; Jiao, J.; Guo, R.; Yang, Y.; Dong, W.; Mi, H.; Wang, M.; Liu, M.; et al. α-Hemihydrate calcium sulfate/n-hydroxyapatite combined with metformin promotes osteogenesis in vitro and in vivo. *Front. Bioeng. Biotechnol.* **2022**, *10*, 899157. [CrossRef]
21. Nauth, A.; Lane, J.; Watson, J.T.; Giannoudis, P. Bone Graft Substitution and Augmentation. *J. Orthop. Trauma* **2015**, *29* (Suppl. S12), S34–S38. [CrossRef]
22. Portnov, T.; Shulimzon, T.; Zilberman, M. Injectable hydrogel-based scaffolds for tissue engineering applications. *Rev. Chem. Eng.* **2017**, *33*, 91–107. [CrossRef]
23. Perez, R.A.; Kim, H.-W.; Ginebra, M.-P. Polymeric additives to enhance the functional properties of calcium phosphate cements. *J. Tissue Eng.* **2012**, *3*, 2041731412439555. [CrossRef]

24. Moreira, C.D.F.; Carvalho, S.M.; Florentino, R.M.; França, A.; Okano, B.S.; Rezende, C.M.; Mansur, H.S.; Pereira, M.M. Injectable chitosan/gelatin/bioactive glass nanocomposite hydrogels for potential bone regeneration: In vitro and in vivo analyses. *Int. J. Biol. Macromol.* **2019**, *132*, 811–821. [CrossRef]
25. Kantak, M.N.; Bharate, S.S. Analysis of clinical trials on biomaterial and therapeutic applications of chitosan: A review. *Carbohydr. Polym.* **2022**, *278*, 118999. [CrossRef]
26. Kean, T.; Thanou, M. Biodegradation, biodistribution and toxicity of chitosan. *Adv. Drug. Deliv. Rev.* **2010**, *62*, 3–11. [CrossRef] [PubMed]
27. Masson, J.-D.; Thibaudon, M.; Bélec, L.; Crépeaux, G. Calcium phosphate: A substitute for aluminum adjuvants? *Expert Rev. Vaccines* **2017**, *16*, 289–299. [CrossRef] [PubMed]
28. Lin, Y.; Wang, X.; Huang, X.; Zhang, J.; Xia, N.; Zhao, Q. Calcium phosphate nanoparticles as a new generation vaccine adjuvant. *Expert Rev. Vaccines* **2017**, *16*, 895–906. [CrossRef] [PubMed]
29. Niculescu, A.-G.; Grumezescu, A.M. Applications of Chitosan-Alginate-Based Nanoparticles-An Up-to-Date Review. *Nanomaterials* **2022**, *12*, 186. [CrossRef] [PubMed]
30. Wack, A.; Baudner, B.C.; Hilbert, A.K.; Manini, I.; Nuti, S.; Tavarini, S.; Scheffczik, H.; Ugozzoli, M.; Singh, M.; Kazzaz, J.; et al. Combination adjuvants for the induction of potent, long-lasting antibody and T-cell responses to influenza vaccine in mice. *Vaccine* **2008**, *26*, 552–561. [CrossRef] [PubMed]
31. Mallakpour, S.; Azadi, E.; Hussain, C.M. Chitosan, alginate, hyaluronic acid, gums, and β-glucan as potent adjuvants and vaccine delivery systems for viral threats including SARS-CoV-2: A review. *Int. J. Biol. Macromol.* **2021**, *182*, 1931–1940. [CrossRef]
32. Hruschka, V.; Tangl, S.; Ryabenkova, Y.; Heimel, P.; Barnewitz, D.; Möbus, G.; Keibl, C.; Ferguson, J.; Quadros, P.; Miller, C.; et al. Comparison of nanoparticular hydroxyapatite pastes of different particle content and size in a novel scapula defect model. *Sci. Rep.* **2017**, *7*, 43425. [CrossRef]
33. Fox, K.; Tran, P.A.; Tran, N. Recent advances in research applications of nanophase hydroxyapatite. *ChemPhysChem* **2012**, *13*, 2495–2506. [CrossRef] [PubMed]
34. Liu, Z.; Yamada, S.; Otsuka, Y.; Peñaflor Galindo, T.G.; Tagaya, M. Surface modification of hydroxyapatite nanoparticles for bone regeneration by controlling their surface hydration and protein adsorption states. *Dalton Trans.* **2022**, *51*, 9572–9583. [CrossRef] [PubMed]
35. Masouleh, M.P.; Hosseini, V.; Pourhaghgouy, M.; Bakht, M. Calcium Phosphate Nanoparticles Cytocompatibility Versus Cytotoxicity: A Serendipitous Paradox. *Curr. Pharm. Des.* **2017**, *23*, 2930–2951. [CrossRef]
36. Velard, F.; Braux, J.; Amedee, J.; Laquerriere, P. Inflammatory cell response to calcium phosphate biomaterial particles: An overview. *Acta Biomater.* **2013**, *9*, 4956–4963. [CrossRef]
37. Mulay, S.R.; Anders, H.-J. Crystallopathies. *N. Engl. J. Med.* **2016**, *374*, 2465–2476. [CrossRef]
38. Chung, F.H. Quantitative interpretation of X-ray diffraction patterns of mixtures. I. Matrix-flushing method for quantitative multicomponent analysis. *J. Appl. Cryst.* **1974**, *7*, 519–525. [CrossRef]
39. Chen, Y.; Liu, Z.; Jiang, T.; Zou, X.; Lei, L.; Yan, W.; Yang, J.; Li, B. Strontium-Substituted Biphasic Calcium Phosphate Microspheres Promoted Degradation Performance and Enhanced Bone Regeneration. *J. Biomed. Mater. Res. Part A* **2020**, *108*, 895–905. [CrossRef]
40. Bradford, M.M. A Rapid and Sensitive Method for the Quantitation of Microgram Quantities of Protein Utilizing the Principle of Protein-Dye Binding. *Anal. Biochem.* **1976**, *72*, 248–254. [CrossRef]
41. Barradas, A.M.C.; Yuan, H.; van Blitterswijk, C.A.; Habibovic, P. Osteoinductive biomaterials: Current knowledge of properties, experimental models and biological mechanisms. *Eur. Cell Mater.* **2011**, *21*, 407–429; discussion 429. [CrossRef] [PubMed]
42. Fadeeva, I.S.; Teterina, A.Y.; Minaychev, V.V.; Senotov, A.S.; Smirnov, I.V.; Fadeev, R.S.; Smirnova, P.V.; Menukhov, V.O.; Lomovskaya, Y.V.; Akatov, V.S.; et al. Biomimetic Remineralized Three-Dimensional Collagen Bone Matrices with an Enhanced Osteostimulating Effect. *Biomimetics* **2023**, *8*, 91. [CrossRef] [PubMed]
43. Lillie, R.D.; Fullmer, H.M. *Histopathologic Technic and Practical Histochemistry—Front Cover*; McGraw-Hill: San Francisco, CA, USA, 1976; p. 942.
44. Van der Houwen, J.A.M.; Cressey, G.; Cressey, B.A.; Valsami-Jones, E. The effect of organic ligands on the crystallinity of calcium phosphate. *J. Cryst. Growth* **2003**, *249*, 572–583. [CrossRef]
45. Koutsopoulos, S. Synthesis and characterization of hydroxyapatite crystals: A review study on the analytical methods. *J. Biomed. Mater. Res.* **2002**, *62*, 600–612. [CrossRef] [PubMed]
46. Jemli, Y.E.L.; Abdelouahdi, K.; Minh, D.P.; Barakat, A.; Solhy, A. Synthesis and Characterization of Hydroxyapatite and Hydroxyapatite-Based Catalysts. In *Design and Applications of Hydroxyapatite-Based Catalysts*; Wiley Online Library: Hoboken, NJ, USA, 2022; pp. 19–72.
47. Kolmas, J.; Kaflak, A.; Zima, A.; Ślósarczyk, A. Alpha-tricalcium phosphate synthesized by two different routes: Structural and spectroscopic characterization. *Ceram. Int.* **2015**, *41*, 5727–5733. [CrossRef]
48. Yubao, L.; Xingdong, Z.; De Groot, K. Hydrolysis and phase transition of alpha-tricalcium phosphate. *Biomaterials* **1997**, *18*, 737–741. [CrossRef]
49. Li, Y.; Kong, F.; Weng, W. Preparation and characterization of novel biphasic calcium phosphate powders (α-TCP/HA) derived from carbonated amorphous calcium phosphates. *J. Biomed. Mater. Res. Part B Appl. Biomater.* **2009**, *89*, 508–517. [CrossRef]
50. Falk, M.; Miller, A.G. Infrared spectrum of carbon dioxide in aqueous solution. *Vib. Spectrosc.* **1992**, *4*, 105–108. [CrossRef]

51. Rey, C.; Combes, C.; Drouet, C.; Grossin, D.; Bertrand, G.; Soulié, J. 1.11 Bioactive Calcium Phosphate Compounds: Physical Chemistry. In *Comprehensive Biomaterials II.*; Ducheyne, P., Ed.; Elsevier: Oxford, UK, 2017; pp. 244–290. ISBN 978-0-08-100692-4.
52. Rampado, R.; Crotti, S.; Caliceti, P.; Pucciarelli, S.; Agostini, M. Recent Advances in Understanding the Protein Corona of Nanoparticles and in the Formulation of "Stealthy" Nanomaterials. *Front. Bioeng. Biotechnol.* **2020**, *8*, 166. [CrossRef]
53. Bai, X.; Wang, J.; Mu, Q.; Su, G. In Vivo Protein Corona Formation: Characterizations, Effects on Engineered Nanoparticles' Biobehaviors, and Applications. *Front. Bioeng. Biotechnol.* **2021**, *9*, 646708. [CrossRef]
54. Miclăuş, T.; Beer, C.; Chevallier, J.; Scavenius, C.; Bochenkov, V.E.; Enghild, J.J.; Sutherland, D.S. Dynamic Protein Coronas Revealed as a Modulator of Silver Nanoparticle Sulphidation in Vitro. *Nat Commun* **2016**, *7*, 11770. [CrossRef] [PubMed]
55. Mijiritsky, E.; Gardin, C.; Ferroni, L.; Lacza, Z.; Zavan, B. Albumin-impregnated bone granules modulate the interactions between mesenchymal stem cells and monocytes under in vitro inflammatory conditions. *Mater. Sci. Eng. C.* **2020**, *110*, 110678. [CrossRef] [PubMed]
56. Simonffy, L.; Minya, F.; Trimmel, B.; Lacza, Z.; Dobo-Nagy, C. Albumin-Impregnated Allograft Filling of Surgical Extraction Sockets Achieves Better Bone Remodeling Than Filling with Either Blood Clot or Bovine Xenograft. *Int. J. Oral Maxillofac. Implant.* **2020**, *35*, 297–304. [CrossRef] [PubMed]